First-principles accurate total-energy surfaces for polar structural distortions of $BaTiO_3$, $PbTiO_3$, and $SrTiO_3$: consequences to structural transition temperatures

Takeshi Nishimatsu[1], Masaya Iwamoto[1], Yoshiyuki Kawazoe[1], and Umesh V. Waghmare[2]
[1] *Institute for Materials Research (IMR), Tohoku University, Sendai 980-8577, Japan*
[2] *Theoretical Sciences Unit, Jawaharlal Nehru Centre for Advanced Scientific Research (JNCASR), Jakkur, Bangalore, 560 064, India*

Specific forms of the exchange correlation energy functionals in first-principles density functional theory-based calculations, such as the local density approximation (LDA) and generalized-gradient approximations (GGA), give rise to structural lattice parameters with typical errors of -2 % and 2 %. Due to a strong coupling between structure and polarization, the order parameter of ferroelectric transitions, they result in large errors in estimation of temperature dependent ferroelectric structural transition properties. Here, we employ a recently developed GGA functional of Wu and Cohen [Phys. Rev. B, **73**, 235116 (2006)] and determine total-energy surfaces for zone-center distortions of $BaTiO_3$, $PbTiO_3$, and $SrTiO_3$, and compare them with the ones obtained with calculations based on standard LDA and GGA. Confirming that the Wu and Cohen functional allows better estimation of structural properties at 0 K, we determine a new set of parameters defining the effective Hamiltonian for ferroelectric transition in $BaTiO_3$. Using the new set of parameters, we perform molecular-dynamics (MD) simulations under effective pressures $p = 0.0$ GPa, $p = -2.0$ GPa, and $p = -0.005T$ GPa. The simulations under $p = -0.005T$ GPa, which is for simulating thermal expansion, show a clear improvement in the cubic to tetragonal transition temperature and c/a parameter of its ferroelectric tetragonal phase, while the description of transitions at lower temperatures to orthorhombic and rhombohedral phases is marginally improved. Our findings augur well for use of Wu-Cohen functional in studies of ferroelectrics at nano-scale, particularly in the form of epitaxial films where the properties depend crucially on the lattice mismatch.

PACS numbers: 64.60.De, 77.80.B-, 77.84.-s

I. INTRODUCTION

It is well known that first-principles density functional theory based calculations within the local density approximation (LDA) underestimate lattice constants slightly (1–2%), and consequently calculated double-well total-energy surfaces[1,2] for ferroelectric structural distortions of ABO_3 perovskite-type ferroelectrics are shallower giving the theoretical transitions temperatures much lower than their observed values (T_C = 403 K = 0.0347 eV for $BaTiO_3$, for example)[3]. In Monte-Carlo (MC) simulations[4] and molecular-dynamics (MD) simulations[5] of $BaTiO_3$, a perovskite-type ferroelectric, an effective Hamiltonian[1,4] constructed from LDA calculations was used. To overcome the limitation of underestimation of lattice constant, these simulations were carried out with a negative pressure of -5 GPa. Similarly, Monte Carlo simulations for $PbTiO_3$ were carried out with an effective Hamiltonian[6] constructed from LDA calculations at the experimental lattice constant. However, both of these schemes resulted in underestimation of T_C.

There are two main sources of errors in estimation of T_C in such simulations: (a) neglect of anharmonic coupling between soft modes and higher energy phonons in construction of effective Hamiltonian, and (b) those arising from underestimation of lattice constants in DFT calculations. While the former was assessed to be small in earlier work[7] and can be partly corrected using a T-dependent pressure to yield a correct thermal expansion, a systematic investigation of the latter would be useful in planning and evaluating future first-principles simulations of ferroelectrics.

To overcome the limitation of DFT calculations in estimation of structural parameters in ferroelectrics, Wu and Cohen introduced a new flavor of generalized gradient approximation (GGA), and obtained an excellent agreement between calculated and experimentally observed lattice constants at zero Kelvin for $PbTiO_3$ and $BaTiO_3$[8]. Recent theoretical works[9,10] further strengthened that the Wu and Cohen functional gives acceptable structural properties of ABO_3 ferroelectrics such as lattice constants, c/a ratio, atomic displacements, phonon frequencies, Born effective charges, etc.

Here, we use the Wu and Cohen GGA-functional and determine possibly more realistic total-energy surfaces of polar distortions of $BaTiO_3$, $PbTiO_3$, and $SrTiO_3$ than those from LDA calculations. Further, we construct an effective Hamiltonian for $BaTiO_3$ with a set of parameters determined from first-principles calculations based on Wu-Cohen functional, and estimate the three of its transition temperatures, and temperature dependent structural properties. Through comparison with transitions properties obtained with the LDA-based effective Hamiltonian and from experiment, we evaluate the efficacy of Wu-Cohen functional in determination of finite-temperature properties.

In Sec. II, we describe the formalism of methods used in computations, with a focus on details of the procedure for determination of the set of parameters of the effective Hamiltonian, which is slightly different from the

earlier works[4,6]. In Sec. III, we present a comparative analysis of calculated total-energy surfaces of $BaTiO_3$, $PbTiO_3$, and $SrTiO_3$ and include results of MD simulations of $BaTiO_3$, and finally summarize our work and conclusions in Sec. IV.

II. METHODS OF CALCULATION AND FORMALISM

A. First-principles methods

All calculations are performed with ABINIT code[11,12]. Bloch wave functions of electrons are expanded in terms of plane waves with a cut-off energy of 60 Hartree, and are sampled on an 8×8×8 grid of k-points in the first Brillouin zone. We use different choices of exchange correlation energy functionals. For LDA calculations, we use the one parametrized by Teter[13] along with Teter's extended norm-conserving pseudopotentials[14]. For GGA calculations, we use "PBE"[15] and "Wu and Cohen"[8] functionals, along with Rappe's optimized pseudopotentials[16] generated with Opium code[17] and compare their results.

B. Total-energy surface

In 1994, King-Smith and Vanderbilt studied the total-energy surface for zone-center distortions of perovskite-type ferroelectric oxides ABO_3 at zero temperature using first-principles calculations with ultrasoft-pseudopotentials and a plane-wave basis set.[1] Starting from the centrosymmetric cubic perovskite structure, and using the normalized Γ_{15} soft-mode eigenvector $\boldsymbol{\xi}_\alpha$ ($= \boldsymbol{\xi}_x = \boldsymbol{\xi}_y = \boldsymbol{\xi}_z$, due to the cubic symmetry) of the interatomic force constant (IFC) matrix[18], they define displacements v_α^τ of atoms τ (=A, B, O_I, O_{II}, O_{III}) in the Cartesian directions $\alpha(= x, y, z)$ as

$$\boldsymbol{v}_\alpha = \begin{pmatrix} v_\alpha^A \\ v_\alpha^B \\ v_\alpha^{O_I} \\ v_\alpha^{O_{II}} \\ v_\alpha^{O_{III}} \end{pmatrix} = u_\alpha \boldsymbol{\xi}_\alpha = u_\alpha \begin{pmatrix} \xi_\alpha^A \\ \xi_\alpha^B \\ \xi_\alpha^{O_I} \\ \xi_\alpha^{O_{II}} \\ \xi_\alpha^{O_{III}} \end{pmatrix} , \qquad (1)$$

with the scalar soft-mode amplitude u_α. Under the condition that the strain components η_i ($i = 1, \cdots, 6$; Voigt notation; $\eta_1 = e_{xx}$, $\eta_4 = e_{yz}$) minimize the total energy for each $\boldsymbol{u} = (u_x, u_y, u_z)$, they expressed the total energy as

$$E^{\rm tot} = E^0 + \kappa u^2 + \alpha' u^4 + \gamma'(u_x^2 u_y^2 + u_y^2 u_z^2 + u_z^2 u_x^2) \ , \quad (2)$$

where $u^2 = u_x^2 + u_y^2 + u_z^2$, E^0 is the total energy of the cubic structure, κ is half the eigenvalue of the Γ_{15} soft mode, and α' and γ' are anharmonic coefficients including the contribution of relaxation of strain through its coupling with atomic displacements. Similar analysis is used in

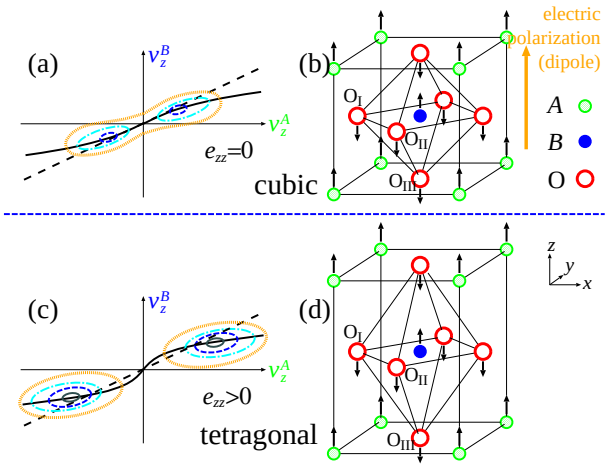

FIG. 1. (Color online) Total-energy surfaces for zone-center distortions of a ferroelectric ABO_3 perovskite on a two-dimensional subspace (v_z^A, v_z^B) of the atomic-displacement space $(v_z^A, v_z^B, v_z^{O_I}, v_z^{O_{II}}, v_z^{O_{III}})$. (a) Schematic contour plot for atomic displacements from the centrosymmetric cubic structure (b), $e_{zz} = 0$, is compared to (c) that from the tetragonal structure (d), $e_{zz} > 0$. Thick solid lines are the valley lines for fixed e_{zz}'s. Dashed lines show the direction of the Γ_{15} soft-mode eigenvector $\boldsymbol{\xi}$ at zero strain. Note that the direction is tangential to the valley line at $v_z^\tau = 0$ for $e_{zz} = 0$, but this is not the case for $e_{zz} \neq 0$.

constructions of effective Hamiltonian in Refs. 4 and 6, which assumes that anharmonic coupling between soft modes and other IR-active modes is vanishingly small.

In 2004, Hashimoto, Nishimatsu *et al.* included some of these anharmonic effects by redefining u_α as

$$u_\alpha = \sqrt{(v_\alpha^A)^2 + (v_\alpha^B)^2 + \left(v_\alpha^{O_I}\right)^2 + \left(v_\alpha^{O_{II}}\right)^2 + \left(v_\alpha^{O_{III}}\right)^2} \ , \qquad (3)$$

and developed automatic computational method to determine valley line of the total-energy surface in the 15-dimensional coordinate space of atomic displacements[2] (See Fig. 1). This method reveals that normalized "direction" $\boldsymbol{\xi}$ of the atomic displacements from the centrosymmetric cubic phase to the distorted minima is not constant as in Eq. (2), but a function of $\boldsymbol{u}$, i.e. $\boldsymbol{\xi}(\boldsymbol{u})$, and the total-energy surface generally cannot be expressed with a 4th order function of atomic displacement amplitude $\boldsymbol{u}$ as in Eq. (2). $\boldsymbol{\xi}(\boldsymbol{u})$ is determined by minimizing energy with respect to all atomic displacements $\{v_\alpha^\tau\}$ such that $\{u_\alpha\}$ in Eq. (3) is fixed. In this paper, we employ this valley line tracing method as implemented in the Patched ABINIT version 5.7.3 to determine accurate total-energy surfaces. The patch file for ABINIT is in the EPAPS[19]. The valley lines can be also calculated under any positive or negative pressure, through use of enthalpy $H = E + pV$ and correspondingly the enthalpy differences $H - H^0$ should be compared rather than total energy $E - E^0$.

C. Effective Hamiltonian

The effective Hamiltonian constructed from first-principles calculations and used in MD simulations is basically the same as that in Ref. 5 and 6,

$$\begin{aligned} H^{\rm eff} = & \frac{M^*_{\rm dipole}}{2}\sum_{\boldsymbol{R},\alpha}\dot{u}^2_\alpha(\boldsymbol{R}) + \frac{M^*_{\rm acoustic}}{2}\sum_{\boldsymbol{R},\alpha}\dot{w}^2_\alpha(\boldsymbol{R}) \\ & + V^{\rm self}(\{\boldsymbol{u}\}) + V^{\rm dpl}(\{\boldsymbol{u}\}) + V^{\rm short}(\{\boldsymbol{u}\}) \\ & + V^{\rm elas,\,homo}(\eta_1,\cdots,\eta_6) + V^{\rm elas,\,inho}(\{\boldsymbol{w}\}) \\ & + V^{\rm coup,\,homo}(\{\boldsymbol{u}\},\eta_1,\cdots,\eta_6) + V^{\rm coup,\,inho}(\{\boldsymbol{u}\},\{\boldsymbol{w}\}) \\ & - Z^*\sum_{\boldsymbol{R}}\boldsymbol{\mathcal{E}}\cdot\boldsymbol{u}(\boldsymbol{R})\ . \end{aligned} \tag{4}$$

Detailed explanation of symbols in the effective Hamiltonian can be found in Refs. 1, 4, and 5. We newly introduced 6th-order terms with coefficients k_1, k_2, and k_3 and an 8th-order term $k_4u^8(\boldsymbol{R})$ to the local-mode self-energy $V^{\rm self}(\{\boldsymbol{u}\})$ as

$$\begin{aligned} V^{\rm self}(\{\boldsymbol{u}\}) = & \sum_{\boldsymbol{R}}\Big\{\kappa_2u^2(\boldsymbol{R}) + \alpha u^4(\boldsymbol{R}) \\ & + \gamma\left[u^2_y(\boldsymbol{R})u^2_z(\boldsymbol{R}) + u^2_z(\boldsymbol{R})u^2_x(\boldsymbol{R}) + u^2_x(\boldsymbol{R})u^2_y(\boldsymbol{R})\right] \\ & + k_1u^6(\boldsymbol{R}) + k_2\big[u^4_x(\boldsymbol{R})(u^2_y(\boldsymbol{R}) + u^2_z(\boldsymbol{R})) \\ & + u^4_y(\boldsymbol{R})(u^2_z(\boldsymbol{R}) + u^2_x(\boldsymbol{R})) + u^4_z(\boldsymbol{R})(u^2_x(\boldsymbol{R}) + u^2_y(\boldsymbol{R}))\big] \\ & + k_3u^2_x(\boldsymbol{R})u^2_y(\boldsymbol{R})u^2_z(\boldsymbol{R}) + k_4u^8(\boldsymbol{R})\Big\}\ , \end{aligned} \tag{5}$$

where $u^2(\boldsymbol{R}) = u^2_x(\boldsymbol{R}) + u^2_y(\boldsymbol{R}) + u^2_z(\boldsymbol{R})$. We introduced this 6th-order terms to follow-up the total-energy surface precisely. The 8th-order term is for preventing the $|\boldsymbol{u}| \to \infty$ breakdown under negative k_1.

In next sections II D and II E, we explain how to determine the parameters for the effective Hamiltonian of Eq. (4) in detail.

D. Elastic coefficients and total-energy surface

Elastic constants expressed in energy unit $B_{11} = a_0^3C_{11}$ and $B_{12} = a_0^3C_{12}$, where a_0 is the equilibrium lattice constant in cubic structure, can be calculated by deforming the cubic unit cell of ABO_3 with strain tensors

$$\overleftrightarrow{\epsilon} = \begin{pmatrix} \delta & 0 & 0 \\ 0 & \delta & 0 \\ 0 & 0 & \delta \end{pmatrix} \tag{6}$$

and

$$\overleftrightarrow{\epsilon} = \begin{pmatrix} 0 & 0 & 0 \\ 0 & 0 & 0 \\ 0 & 0 & \delta \end{pmatrix}\ . \tag{7}$$

Deformation in Eq. (6) alters the total energy from its equilibrium value E^0 by

$$E(\delta) = E^0 + \frac{3}{2}(B_{11} + 2B_{12})\delta^2 + O(\delta^4)\ . \tag{8}$$

More precisely, volume dependence of total energy may be fitted with the Birch-Murnaghan equation of state[20–22]. Deformation in Eq. (7) gives

$$E(\delta) = E^0 + \frac{1}{2}B_{11}\delta^2 + O(\delta^4)\ . \tag{9}$$

For $B_{44} = a_0^3C_{44}$, deformation

$$\overleftrightarrow{\epsilon} = \begin{pmatrix} 0 & \delta & \delta \\ \delta & 0 & \delta \\ \delta & \delta & 0 \end{pmatrix} \tag{10}$$

and

$$E(\delta) = E^0 + \frac{3}{2}B_{44}\delta^2 + O(\delta^4) \tag{11}$$

can be used.

B_{1xx}, B_{1yy}, and B_{4yz}, the coupling coefficients defined in Ref. 1, are determined from quadratic u dependence of strain. In the case of [110] distortion (see Fig. 2(e), for example),

$$e_{xx} = a_{xx}u^2 \tag{12a}$$

$$e_{xy} = a_{xy}u^2 \tag{12b}$$

$$e_{zz} = a_{zz}u^2 \tag{12c}$$

emerge

$$B_{1xx} = -4B_{11}a_{xx} + 2(B_{11} - 2B_{12})a_{zz} \tag{13a}$$

$$B_{1yy} = -4B_{12}a_{xx} - 2B_{11}a_{zz} \tag{13b}$$

$$B_{4yz} = -2B_{44}a_{xy}\ . \tag{13c}$$

Anharmonic coefficients in the on-site energy α, γ, k_1, k_2, k_3, and k_4 in Eq. (5) are determined from u-dependences of total energies of [001], [110], and [111] distortions as

$$E_{001}(u) = \kappa u^2 + \alpha' u^4 + k_1u^6 + k_4u^8, \tag{14a}$$

$$E_{110}(u) = \kappa u^2 + (\alpha' + \frac{1}{4}\gamma')u^4 + (k_1 + \frac{1}{4}k_2)u^6 + k_4u^8, \tag{14b}$$

$$\begin{aligned} E_{111}(u) = & \kappa u^2 + (\alpha' + \frac{1}{3}\gamma')u^4 \\ & + (k_1 + \frac{2}{9}k_2 + \frac{1}{27}k_3)u^6 + k_4u^8\ . \end{aligned} \tag{14c}$$

With Eq. (19a) and (19b) in Ref. 1, α' and γ' can be converted into α and γ. It should be mentioned that it is quite difficult to express the total-energy surfaces even with up to 8th order polynomial in wide range of u. Therefore, we fit Eqs. (14a)–(14c) only to the calculated data points within narrow range of u, e.g. $|u| \le 0.3$ [Å] for $BaTiO_3$.

E. Response-function calculations

We perform some response-function (RF) calculations[18] with ABINIT, determine IFC matrices at the $\boldsymbol{k}$-points of Γ, X, M, R, and center of the Σ

axis (See Fig. 3(A)), then calculate their eigenvalues and eigenvectors.

We can determine local and short-range interaction parameters κ_2 and $j_1, \cdots, j_7$ in Ref. 4 from selected eigenvalues $2\kappa(\Gamma_{\rm TO})$, $2\kappa(\rm X_1)$, $2\kappa(\rm X_5)$, $2\kappa(\rm M_{3'})$, $2\kappa(\rm M_{5'})$, $2\kappa(\rm R_{25'})$, and $2\kappa(\Sigma_{\rm LO})$. Here, it is emphasised that $\kappa(\boldsymbol{k}_i)$ is *half* of the mode-i eigenvalue $2\kappa(\boldsymbol{k}_i)$ of the IFC matrix at each $\boldsymbol{k}$-point. Practically, κ_2 and $j_1, \cdots, j_7$ are determined by solving linear equation as described in Ref. 4, in CGS units,

$$\kappa(\Gamma_{\rm TO}) = -\frac{2}{3}\pi\frac{Z^{*2}}{\epsilon_\infty a_0^3} + \kappa_2 + 2j_1 + j_2 + 4j_3 + 2j_4 + 4j_6 \quad (15a)$$

$$\kappa(\rm X_1) = 4.84372\frac{Z^{*2}}{\epsilon_\infty a_0^3} + \kappa_2 + 2j_1 - j_2 - 4j_3 + 2j_4 - 4j_6 \quad (15b)$$

$$\kappa(\rm X_5) = -2.42186\frac{Z^{*2}}{\epsilon_\infty a_0^3} + \kappa_2 + j_2 - 2j_4 - 4j_6 \quad (15c)$$

$$\kappa(\rm M_{3'}) = -2.67679\frac{Z^{*2}}{\epsilon_\infty a_0^3} + \kappa_2 - 2j_1 + j_2 - 4j_3 + 2j_4 + 4j_6 \quad (15d)$$

$$\kappa(\rm M_{5'}) = 1.33839\frac{Z^{*2}}{\epsilon_\infty a_0^3} + \kappa_2 - j_2 - 2j_4 + 4j_6 \quad (15e)$$

$$\kappa(\rm R_{25'}) = \kappa_2 - 2j_1 - j_2 + 4j_3 + 2j_4 - 4j_6 \quad (15f)$$

$$\kappa(\Sigma_{\rm LO}) = 2.93226\frac{Z^{*2}}{\epsilon_\infty a_0^3} + \kappa_2 + j_1 - 2j_5 - 4j_7\ , \quad (15g)$$

and

$$0 = j_6 - j_7\ . \quad (16)$$

Moreover, we newly assume that $j_5 = 0$ and $j_7 = 0$. With this assumption, we can omit one RF calculation for the center of the Σ axis, and we do not use Eq. (15g) and Eq. (16). We can employ this assumption because j_5 and j_7 do not affect low energy polarization modes.

There may be an inconsistency between κ from Eqs. (14a)–(14c) and $\kappa(\Gamma_{\rm TO})$ in Eq. (15a). To keep the total-energy surfaces unchanged, κ from Eqs. (14a)–(14c) should be adopted. Therefore, We add the difference between κ and $\kappa(\Gamma_{\rm TO})$ to κ_2 as

$$\kappa_2 \leftarrow \kappa_2 + [\kappa - \kappa(\Gamma_{\rm TO})]\ . \quad (17)$$

This correction can be employed, because correction of κ_2 just leads parallel elevation of dispersion, e.g. Fig. 3(B).

From the calculated normalized Γ_{15} soft-mode eigenvector $\boldsymbol{\xi}_\alpha$, we determine the Born effective charge Z^* and the effective mass $M^*_{\rm dipole}$ of the soft mode. For Z^*, we also use the calculated effective charge tensor $Z^{*\tau}_{zz}$ for each atom τ,

$$Z^* = \sum_\tau \xi_z^\tau\ Z^{*\tau}_{zz}\ . \quad (18)$$

The effective mass will be

$$M^*_{\rm dipole} = \sum_\tau \{\xi_z^\tau\}^2 M^\tau\ , \quad (19)$$

where M^τ is the mass of atom τ.

The optical dielectric constant ϵ_∞ can be also determined in RF calculations.

F. Conditions of molecular-dynamics simulations

MD simulations for $BaTiO_3$ with the effective Hamiltonian of Eq. (4) are performed with our original MD code `feram` (`http://loto.sourceforge.net/feram/`). Details of the code can be found in Ref. 5. Temperature is kept constant in each temperature step in the canonical ensemble using the Nosé-Poincaré thermostat.[23] This simplectic thermostat is so efficient that we can set the time step to $\Delta t = 2$ fs. In our present MD simulations, we thermalize the system for 180,000 time steps, after which we average the properties for 20,000 time steps. We used a supercell of system size $L_x \times L_y \times L_z = 14 \times 14 \times 14$ and small temperature steps in heating-up (+1 K/step) and cooling-down (−1 K/step) simulations. It should be noted that the larger supercell size and the more rapid heating-up and cooling-down result in the larger temperature hysteresis. The initial configuration are generated randomly: $\langle u_\alpha \rangle = 0.11$ Å and $\langle u_\alpha^2 \rangle - \langle u_\alpha \rangle^2 = (0.02\ \text{Å})^2$. We have checked that there is no dependence of results of these simulations on initial configurations.

TABLE I. Calculated equilibrium lattice constants a_0 for cubic phases are compared to experimental values observed just above T_C. Experimental values are cited from Refs. 24 and 3 for $BaTiO_3$ ($T_C = 403$ K), Ref. 25 for $PbTiO_3$ ($T_C = 763$ K), and Ref. 26 for $SrTiO_3$ ($T_C = 106$ K).

	$BaTiO_3$	$PbTiO_3$	$SrTiO_3$
experiment	4.010 Å	3.960 Å	3.896 Å
LDA (Teter)	3.938 Å	3.880 Å	3.845 Å
GGA (PBE)	4.034 Å	3.976 Å	3.946 Å
GGA (W&C)	3.986 Å	3.930 Å	3.901 Å
LDA under	3.989 Å	3.905 Å	3.899 Å
negative pressure	−7.0 GPa	−4.0 GPa	−8.0 GPa

III. RESULTS AND DISCUSSION

Calculated total-energy curves along [001], [110], and [111] distortion directions of $BaTiO_3$ with three functionals are shown in Fig. 2. It is clear that LDA results in shallow double wells and GGA (PBE) results in rather deep wells, while GGA (Wu and Cohen) results in intermediate depths of the double well potentials. Note that, in Fig. 2(a), double wells of LDA results cannot be recognized in this scale of energy. It can be said that GGA (Wu and Cohen) succeeds in reproducing total-energy surfaces at 0 K. These results can be understood from estimated equilibrium cubic lattice constants $a_0 =$ 3.938, 4.034, and 3.986 Å, respectively (See also Table I.). GGA (Wu and Cohen) results also reveal that the "direction" $\boldsymbol{\xi}(\boldsymbol{u})$ of atomic displacements largely depends on u, as shown in Fig. 2(f) even in $BaTiO_3$, which exhibits relatively small polar structural distortions across its ferroelectric transition. For emphasizing that the depth of the double wells are strongly affected by equilibrium cubic lattice constant, total-energy surfaces calculated with LDA under negative pressure −7.0 GPa ($a_0 = 3.989$ Å) are calculated and show in Fig. 2(d). This value of negative pressure, −7.0 GPa, is selected to get similar total-energy surfaces as the GGA (Wu and Cohen) results from $-1.0, -2.0, \cdots, -9.0$ GPa calculations. It can be seen that LDA under certain negative pressure gives results similar to those of GGA (Wu and Cohen).

From our calculations with GGA (Wu and Cohen), i.e. total-energy surfaces, u-dependence of strain (Fig. 2(e)), IFC matrices, etc., we construct a new parameter set of effective Hamiltonian for $BaTiO_3$. The parameters from Refs. 1 and 4 and those of present work are compared in Table II. As shown in Fig. 3(A), without short-range interaction, pure dipole-dipole long-range interaction results in an antiferroelectric cell-doubling state as the most stable structure, corresponding to the strongest instability at M point. However, as shown in Fig. 3(B), introduction of short-range interactions κ_2 and $j_1, \cdots, j_7$ results in the ferroelectric state as the most stable structure at the Γ point.

In Fig. 4, dipole moment per unit cell as a function of

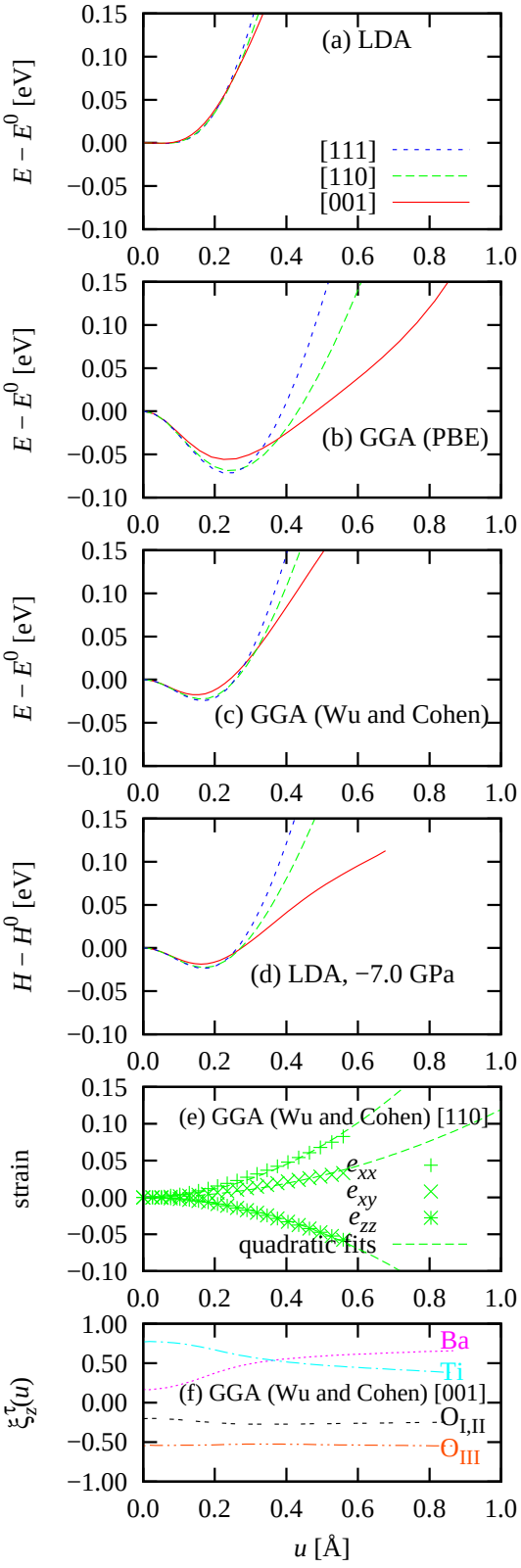

FIG. 2. (Color online) (a)–(d) Total-energy surfaces for zone-center distortions of $BaTiO_3$. (e) u-dependence of strain along [110] distortion. (f) "Direction" $\boldsymbol{\xi}(\boldsymbol{u})$ of atomic displacements along [001] distortion.

TABLE II. Comparison of two set of parameters for the $BaTiO_3$ effective Hamiltonian. "—" indicates that values was not in use. "n.a." indicates that values are not available. p is constant or temperature T [K] dependent effective negative pressures applied while MD simulations. κ in Eqs. (14a)–(14c) and $\kappa(\boldsymbol{k}_i)$ in Eqs. (15a)–(15g) are also listed. They are used to determine κ_2 and $j_1, \cdots, j_7$. ξ_z^τ are the soft-mode eigenvector.

parameter		Refs. 1 and 4	present work
p	[GPa]	-4.8	$-0.005T$
a_0	[Å]	3.95	3.986
B_{11}	[eV]	127.0	126.73
B_{12}	[eV]	44.9	41.76
B_{44}	[eV]	50.3	49.24
B_{1xx}	[eV/Å^2]	$-211.$	-185.35
B_{1yy}	[eV/Å^2]	-19.3	-3.2809
B_{4yz}	[eV/Å^2]	-7.75	-14.550
α	[eV/Å^4]	111.	78.99
γ	[eV/Å^4]	$-164.$	-115.48
k_1	[eV/Å^6]	—	-267.98
k_2	[eV/Å^6]	—	197.50
k_3	[eV/Å^6]	—	830.20
k_4	[eV/Å^8]	—	641.97
m^*	[amu]	—	38.24
Z^*	[e]	9.956	10.33
ϵ_∞		5.24	6.87
κ_2	[eV/Å^2]	5.52	8.534
j_1	[eV/Å^2]	-2.657	-2.084
j_2	[eV/Å^2]	3.906	-1.129
j_3	[eV/Å^2]	0.901	0.689
j_4	[eV/Å^2]	-0.792	-0.611
j_5	[eV/Å^2]	0.564	0.000
j_6	[eV/Å^2]	0.360	0.277
j_7	[eV/Å^2]	0.180	0.000
κ	[eV/Å^2]	-1.695	-1.518
$\kappa(\Gamma_{\rm TO})$	[eV/Å^2]	n.a.	-1.906
$\kappa(\rm X_1)$	[eV/Å^2]	n.a.	17.128
$\kappa(\rm X_5)$	[eV/Å^2]	n.a.	-1.422
$\kappa(\rm M_{3'})$	[eV/Å^2]	n.a.	-1.143
$\kappa(\rm M_{5'})$	[eV/Å^2]	n.a.	16.333
$\kappa(\rm R_{25'})$	[eV/Å^2]	n.a.	13.871
ξ_z^A		0.20	0.166
ξ_z^B		0.76	0.770
$\xi_z^{\rm O_I}$		-0.21	-0.202
$\xi_z^{\rm O_{II}}$		-0.21	-0.202
$\xi_z^{\rm O_{III}}$		-0.53	-0.546
Z_{zz}^{*A}	[e]	2.75	2.741
Z_{zz}^{*B}	[e]	7.16	7.492
$Z_{zz}^{*\rm O_I}$	[e]	-2.11	-2.150
$Z_{zz}^{*\rm O_{II}}$	[e]	-2.11	-2.150
$Z_{zz}^{*\rm O_{III}}$	[e]	-5.69	-5.933

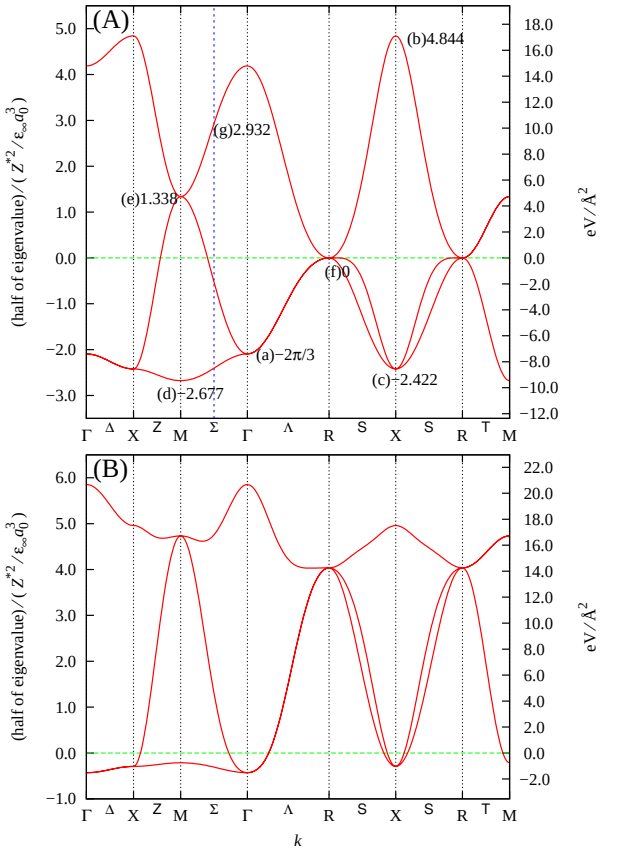

FIG. 3. (Color online) (A) Half of eigenvalues of the 3×3 long-range dipole-dipole interaction matrix $\widetilde{\Phi}(\boldsymbol{k})$ (Fourier transform of Eq. (10) in Ref. 5) are plotted along symmetric axes in the the first Brillouin zone of the simple-cubic lattice. Special points and $\boldsymbol{k}/(2\pi/a) = (\frac{1}{4}, \frac{1}{4}, 0)$ (the center of the Σ axis) are indicated with vertical dotted lines. Labels (a)–(g) corresponds to Eqs. (15a)–(15g), respectively. Tics in the unit of $\frac{Z^{*2}}{\epsilon_\infty a_0^3}$ is placed in left side. Tics in the unit of eV, in the case of the parameter set of Table II, is placed in right side. (B) Half of eigenvalues of the total (long-range + short-range) interaction matrix $\widetilde{\Phi}^{\rm quad}(\boldsymbol{k})$ (Eq. (13) in Ref. 5).

u for atomic displacements along [001] distortion calculated with the Berry-phase theory[27] is shown. As compared with Z^*u, it can be seen that linearity is broken at large u. Since following MD simulations are based in energetics, effects of this nonlinear $Z^*(\boldsymbol{u})$ mainly get folded into anharmonic terms, i.e. α, γ, k_1, k_2, k_3, and k_4. However, still, there might be issues with intersite anharmonic interactions. We leave the issues for future studies.

From the Table II, it is evident that most parameters in the effective Hamiltonian are sensitive to the choice of exchange-correlation functional, with the exception of elastic constants and the mode effective charge. Largest change is seen in the parameters of coupling between strain and polarization, as is expected from the fact that Wu-Cohen functional gives a better estimate of lattice

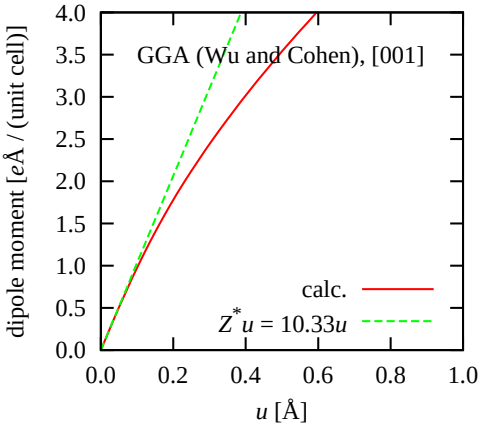

FIG. 4. (Color online) Calculated dipole moment per unit cell as a function of u for atomic displacements along [001] distortion (solid line). Z^*u is also plotted for comparison (dashed line).

parameters and that they couple strongly with polarization. Electronic contribution to the dielectric constant ϵ_∞ is further overestimated with Wu-Cohen functional (it is typically 20 % overestimated in an LDA-based calculation). Due to the use of Hashimoto-Nishimatsu's valley tracing technique, description of the on-site potential energy curve requires anharmonic terms expanded up to 8th order.

Using the Wu-Cohen functional-based parametrized effective Hamiltonian, we perform heating-up and cooling-down MD simulations. In Fig. 5, lattice parameters as functions of temperature are plotted under (a) p = 0.0 GPa, (b) $p = -2.0$ GPa, and (c) $p = -0.005T$ GPa, where T is the temperature in Kelvin. $p = -2.0$ GPa and $p = -0.005T$ are used to obtain a lattice constant of 4.010 Å just above $T_C = 403$ K. Note that, at $T = 400$ K, $p = -0.005T = -2.0$ GPa. The latter temperature-dependent effective negative pressure is for simulating thermal expansion.[28,29] We note that adjustment of the lattice constant through a negative pressure(s) results in significant improvement in the temperature of transition from cubic to tetragonal phase, while the description of the lower two transitions improves only slightly. Results with Wu-Cohen functional (in all the three schemes, 0.0, −2.0, and $-0.005T$ GPa pressures) show a significant improvements in cubic-to-tetragonal transition temperature compared to the LDA-based results of previous MC[4] and MD[5] calculations, but not in the lower two transitions. These mal-improvements in the lower two transitions may be coming from difficulties in accurate first-principles calculations and polynomial fittings of almost degenerated bottom of double wells of [001], [110], and [111] distortions. In Table III, simulated transition temperatures are compared to the previous MD simulations[5] with LDA-based parameters and experimentally observed values. Comparing them to experimentally observed temperature dependence of lattice parameters in Ref. 24, we also note that $p = -0.005T$ GPa gives better temperature dependence of c/a of tetragonal phase than $p = 0.0$ or $p = -2.0$ GPa, though c/a is still slightly overestimated.

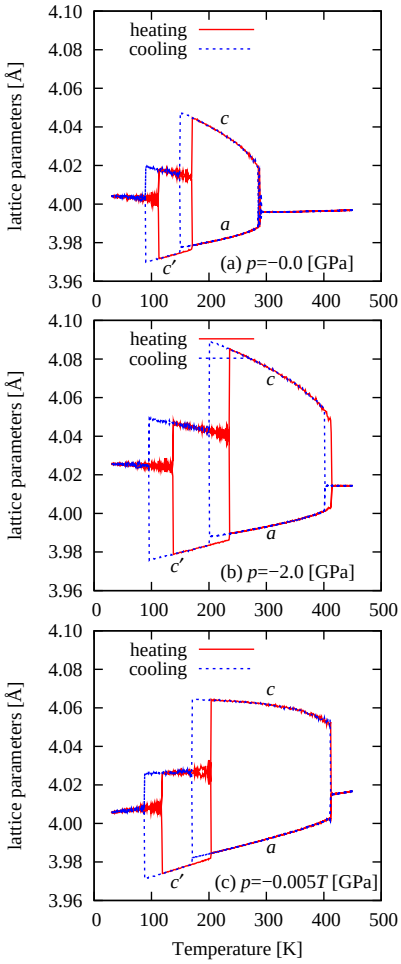

FIG. 5. (Color online) Simulated temperature dependence of lattice parameters under (a) p = −0.0 GPa, (b) p = −2.0 GPa, (c) $p = -0.005T$ GPa.

We also calculated total-energy surfaces for zone-center distortions of $PbTiO_3$ and $SrTiO_3$ in Figs. 6 and 7, respectively. Note that $SrTiO_3$ is not a ferroelectric material and the polarizing zone-center distortion is not to be realized. However, these may be useful data for investigating epitaxial constraint $SrTiO_3$ films where the polarization properties depend crucially on the lattice mismatch. In both cases, similar trends in energetics as those in $BaTiO_3$ can be seen: LDA results in shallow double wells and GGA (PBE) results in rather deep wells, while GGA (Wu and Cohen) results in intermediate depths of the double well potentials. Again, LDA calculations under negative pressures, −4.0 GPa for $PbTiO_3$ and −8.0 GPa for $SrTiO_3$, give similar results to those of GGA (Wu and Cohen). Equilibrium cubic lattice constants are compared in Table I.

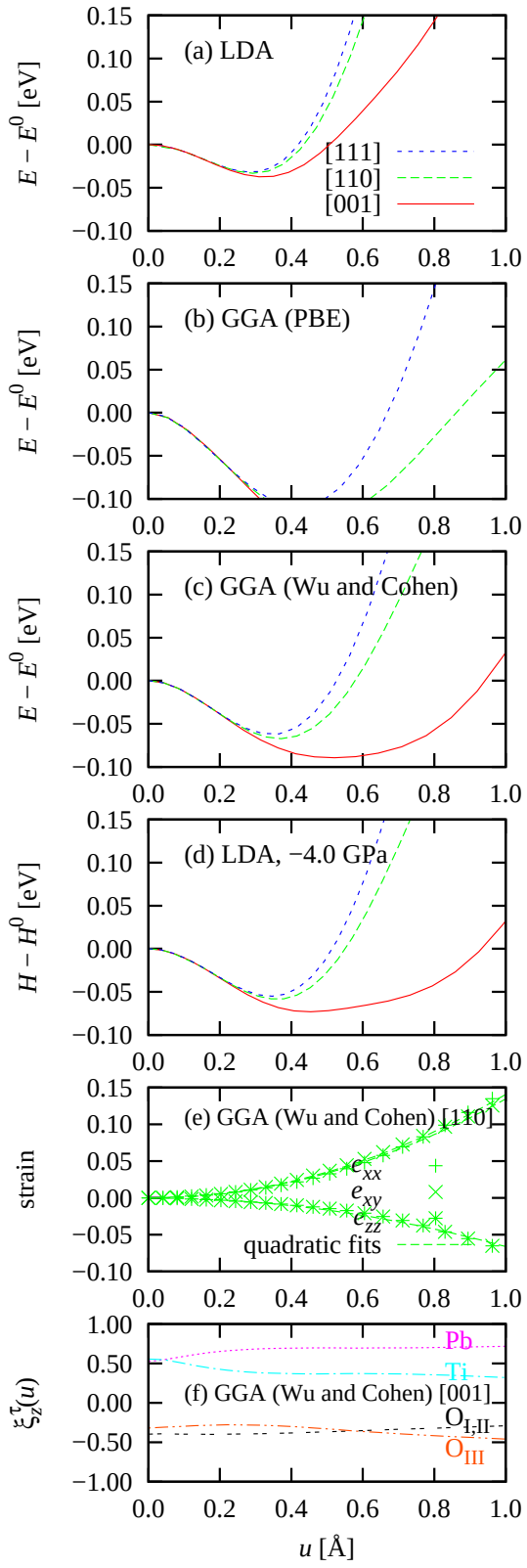

FIG. 6. (Color online) (a)–(d) Total-energy surfaces for zone-center distortions of $PbTiO_3$. (e) u-dependence of strain along [110] distortion. (f) "Direction" $\boldsymbol{\xi}(\boldsymbol{u})$ of atomic displacements along [001] distortion.

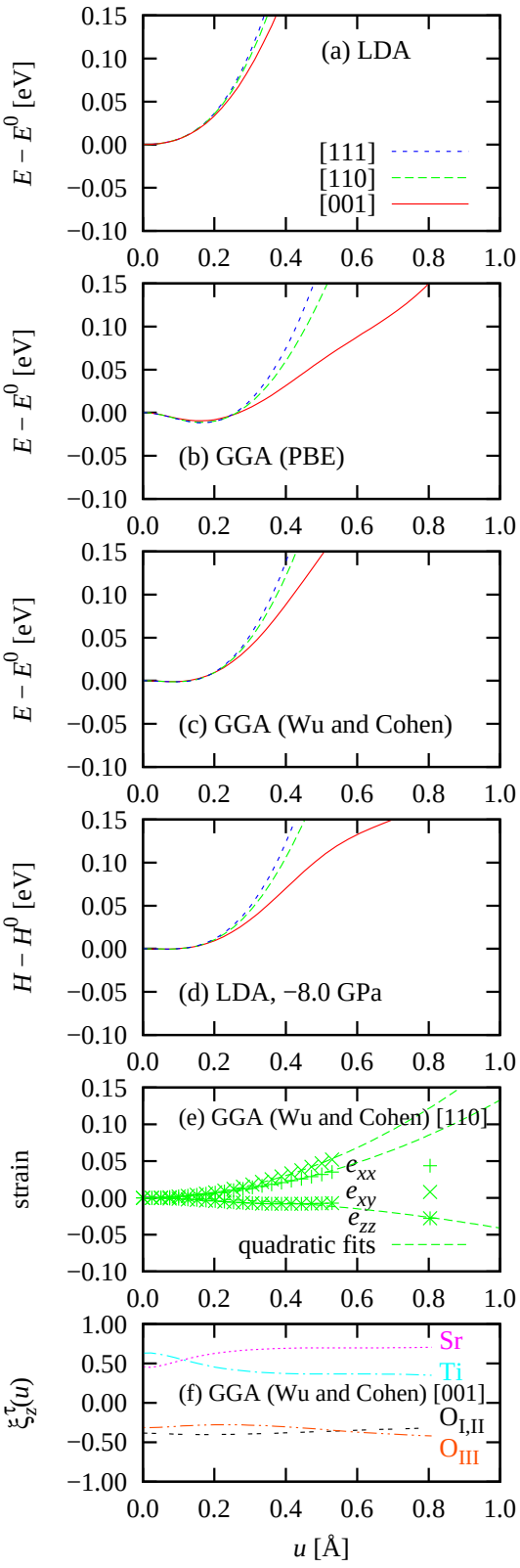

FIG. 7. (Color online) (a)–(d) Total-energy surfaces for zone-center distortions of $SrTiO_3$. (e) u-dependence of strain along [110] distortion. (f) "Direction" $\boldsymbol{\xi}(\boldsymbol{u})$ of atomic displacements along [001] distortion.

TABLE III. Simulated cubic ↔ tetragonal, tetragonal ↔ orthorhombic, and orthorhombic ↔ rhombohedral transition temperatures are compared to the previous MD simulations[5] with LDA-based parameters and experimentally observed values. Heating-up and cooling-down transition temperatures are averaged when corresponding transition has temperature hysteresis.

XC functional and effective negative pressure	ortho. rhombo.	tetra. ortho.	cubic tetra.
GGA (W&C), 0.0 GPa	102 K	160 K	288 K
GGA (W&C), −2.0 GPa	117 K	218 K	408 K
GGA (W&C), $-0.005T$ GPa	103 K	187 K	411 K
LDA, 0.0 GPa	95 K	110 K	137 K
LDA, −5.0 GPa	210 K	245 K	320 K
experiment (after Refs. 24 and 3)	183 K	278 K	403 K

IV. SUMMARY

In this work, we have evaluated the improvement in the description of energy surface at 0 K relevant to ferroelectricity in perovskite-based titanates with use of Wu-Cohen GGA functional for exchange correlation energy in first-principles density functional theoretical calculations to correctly estimate lattice constants and crystallographic anisotropy such as c/a ratio. We have demonstrated that the new GGA (Wu and Cohen) functional based calculations and LDA calculations under certain negative pressures are capable of yielding fairly accurate and comparable total-energy surfaces of zone-center distortions for $AB\mathrm{O}_3$ perovskite-type ferroelectrics; BaTiO_3, PbTiO_3, and SrTiO_3. We have shown that their polar structural distortions are highly sensitive to their lattice constants, and hence much of the improvement with Wu-Cohen functional comes from its ability to correctly estimate lattice constants. We note that the use of Wu-Cohen functional has little influence elastic parameters, the soft mode eigenvectors and mode effective charges which govern the long-range dipolar interactions. What is most affected are the terms of the cubic anisotropy, as reflected in the strain coupling term B_{1yy} and anharmoinc terms, and hence in the relative energy well-depths of polar distortions along [001], [110], and [111] directions. This is not quite surprising as the motivation in development of the Wu-Cohen functional was to get structural properties such as c/a ratio and lattice constants with better accuracy.

We then analyzed consequences of this improvement in energy functional to finite temperature ferroelectric transition, taking an example of BaTiO_3. To this end, starting from calculations with GGA (Wu and Cohen) functional, we constructed a new parameter set for effective Hamiltonian of BaTiO_3 employing the valley-tracing technique that effectively includes anharmonic coupling of the soft polar mode with higher energy polar modes. Comparing this and an LDA-based effective Hamiltonian with MD simulations, we find that the use of Wu-Cohen functional leads to a clear improvement in description of the highest temperature transition from cubic to tetragonal phase. We also confirmed that, as already mentioned in Refs. 28 and 29, the effect of thermal expansion, which is basically coming from the odd order energy terms of atomic displacements and their coupling with strains, cannot be ignored as these materials exhibit strong electro-mechanical couplings. Secondly, accounting for thermal expansion approximately through the temperature-dependent effective negative pressure in effective Hamiltonian, a more realistic description of ferroelectric phase transition can be obtained.

ACKNOWLEDGMENTS

Computational resources were provided by the Center for Computational Materials Science, Institute for Materials Research (CCMS-IMR), Tohoku University. We thank the staff at CCMS-IMR for their constant effort. This study was also supported by the Next Generation Super Computing Project, Nanoscience Program, MEXT, Japan. UVW acknowledges an IBM faculty award grant in supporting some of his work.

[1] R. D. King-Smith and D. Vanderbilt, Phys. Rev. B, **49**, 5828 (1994).
[2] T. Hashimoto, T. Nishimatsu, H. Mizuseki, Y. Kawazoe, A. Sasaki, and Y. Ikeda, Jpn. J. Appl. Phys., **43**, 6785 (2004).
[3] C. J. Johnson, Appl. Phys. Lett., **7**, 221 (1965).
[4] W. Zhong, D. Vanderbilt, and K. M. Rabe, Phys. Rev. B, **52**, 6301 (1995).
[5] T. Nishimatsu, U. V. Waghmare, Y. Kawazoe, and D. Vanderbilt, Phys. Rev. B, **78**, 104104 (2008).
[6] U. V. Waghmare and K. M. Rabe, Phys. Rev. B, **55**, 6161 (1997).
[7] K. M. Rabe and U. V. Waghmare, Ferroelectrics, **136**, 147 (1992).
[8] Z. G. Wu and R. E. Cohen, Phys. Rev. B, **73**, 235116 (2006).
[9] D. I. Bilc, R. Orlando, R. Shaltaf, G.-M. Rignanese, J. Íñiguez, and P. Ghosez, Phys. Rev. B, **77**, 165107 (2008).
[10] R. Wahl, D. Vogtenhuber, and G. Kresse, Phys. Rev. B, **78**, 104116 (2008).
[11] X. Gonze, J.-M. Beuken, R. Caracas, F. Detraux, M. Fuchs, G.-M. Rignanese, L. Sindic, M. Verstraete, G. Zerah, F. Jollet, M. Torrent, A. Roy, M. Mikami, P. Ghosez, J.-Y. Raty, and D. C. Allan, Comput. Mater. Sci., **25**, 478 (2002).
[12] X. Gonze, B. Amadon, P.-M. Anglade, J.-M. Beuken, F. Bottin, P. Boulanger, F. Bruneval, D. Caliste, R. Cara-

cas, M. Cote, T. Deutsch, L. Genovese, P. Ghosez, M. Giantomassi, S. Goedecker, D. R. Hamann, P. Hermet, F. Jollet, G. Jomard, S. Leroux, M. Mancini, S. Mazevet, M. J. T. Oliveira, G. Onida, Y. Pouillon, T. Rangel, G.-M. Rignanese, D. Sangalli, R. Shaltaf, M. Torrent, M. J. Verstraete, G. Zerah, and J. W. Zwanziger, Comput. Phys. Commun., **180**, 2582 (2009).

[13] S. Goedecker, M. Teter, and J. Hutter, Phys. Rev. B, **54**, 1703 (1996).

[14] M. Teter, Phys. Rev. B, **48**, 5031 (1993).

[15] J. P. Perdew, K. Burke, and M. Ernzerhof, Phys. Rev. Lett., **77**, 3865 (1996).

[16] A. M. Rappe, K. M. Rabe, E. Kaxiras, and J. D. Joannopoulos, Phys. Rev. B, **41**, 1227 (1990).

[17] *Opium - pseudopotential generation project,* `http://opium.sourceforge.net/` ((2009)).

[18] X. Gonze and C. Lee, Phys. Rev. B, **55**, 10355 (1997).

[19] See EPAPS Document No. XXXXX for `brdmin.2010-03-02.patch`, a patch file for `src/21drive/brdmin.F90` in ABINIT version 5.7.3 and 5.7.4. Input files for [001], [110], and [111] directions are also placed in the same directory. This document can be reached through a direct link in the online article's HTML reference section or via the EPAPS homepage `http://www.aip.org/pubservs/epaps.html` .

[20] F. D. Murnaghan, Proc. Nat. Acad. Sci. U.S.A., **30**, 244 (1944).

[21] F. Birch, Phys. Rev., **71**, 809 (1947).

[22] O. L. Anderson, J. Phys. Chem. Solids, **27**, 547 (1966).

[23] S. D. Bond, B. J. Leimkuhler, and B. B. Laird, J. Comput. Phys., **151**, 114 (1999).

[24] H. F. Kay and P. Vousden, Philosophical Magazine, **40**, 1019 (1949).

[25] G. Shirame, S. Hoshino, and K. Suzuki, Phys. Rev., **80**, 1105 (1950).

[26] A. Okazaki and M. Kawaminami, Mater. Res. Bull., **8**, 545 (1973).

[27] R. D. King-Smith and D. Vanderbilt, Phys. Rev. B, **47**, 1651 (1993).

[28] K. Leung, E. Cockayne, and A. F. Wright, Phys. Rev. B, **65**, 214111 (2002).

[29] S. Tinte, J. Íñiguez, K. M. Rabe, and D. Vanderbilt, Phys. Rev. B, **67**, 064106 (2003).